Geophys. J. Int. (1992) **109,** 481–487

Models of convection-driven tectonic plates: a comparison of methods and results

Scott D. King,[1]* Carl W. Gable[2] and Stuart A. Weinstein[3]†

[1] *IGPP, Scripps Institution of Oceanography, UCSD, La Jolla, CA* 92093, *USA*

[2] *IGPP, Earth and Environmental Sciences, Los Alamos National Laboratory, Los Alamos, NM* 87545, *USA and Department of Earth and Planetary Sciences, Harvard University, Cambridge, MA* 02138, *USA*

[3] *Department of Earth and Planetary Sciences, The Johns Hopkins University, Baltimore, MD* 21218, *USA*

Accepted 1991 November 8. Received 1991 November 6; in original form 1991 June 28

SUMMARY

Recent numerical studies of convection in the Earth's mantle have included various features of plate tectonics. A number of different methods for modelling 'plate-like' behaviour have been used. The differences in the methods of modelling plates may assume or predict significantly different plate deformation. We describe three methods of modelling plates through: material properties, force balance, and a thin power-law sheet approximation. We compare the results obtained using each method on a series of simple calculations. From these results we are able to develop scaling relations between the different parametrizations. While each method produces different degrees of deformation within the surface plate, the surface heat flux and average plate velocity agree to within a few per cent. The main results are not dependent upon the plate modelling method and therefore are representative of the physical system we set out to model.

Key words: convection, Earth's mantle, plate tectonics.

1 INTRODUCTION

A striking and unique feature of the dynamic Earth is that it's surface is divided into tectonic plates (Le Pichon 1968; Morgan 1968). These plates behave like rigid caps on the Earth's surface with surface deformation concentrated at the plate boundaries (e.g., Isacks, Oliver & Sykes 1968). Using boundary layer theory, Turcotte & Oxburgh (1967) demonstrated that cold sinking lithosphere may provide sufficient driving force to move plates at their observed velocities. However, calculations of infinite Prandtl number convection with uniform material properties (e.g., McKenzie, Roberts & Weiss 1974) or temperature-dependent viscosity (e.g., Nataf & Richter 1982) do not exhibit plate-like surface velocities. In general, plate-like surface velocities are only observed in convection calculations with the help of a plate generation method.

There have been a number of investigations of plates in convective solutions and a variety of methods have been used to induce plate-like behaviour (e.g., Richter & McKenzie 1978; Kopitzke 1979; Davies 1988; Gurnis 1988; Gurnis & Hager 1989; King & Hager 1990; Gable, O'Connell & Travis 1991). However, only one brief investigation comparing different methods has been undertaken (Davies 1989). It is difficult to compare results obtained using different methods, because results are often presented in terms of implementation specific parameters. In light of this, two important questions arise: do different methods have essentially the same result on the convective flow, and if so, is it possible to relate the material properties used in the various methods to observables such as heat flux and plate velocity? The importance of understanding the difference between the parametrizations is more than a study of numerical methods since the resulting plates are often quite different. In particular, the deformation of the plate assumed or predicted by different parametrizations can vary from a uniform velocity with no intraplate deformation to a velocity distribution with a broad zone of deformation.

It is important, before we proceed, to present our criterion for judging a convective solution to have plate-like surface velocities. First, we will consider plates which have the same composition as the underlying mantle. Because of this, these plates will more closely resemble oceanic plates than continental plates which are compositionally different from the mantle. Second, plate interiors should have low strain-rates so that the surface velocities are nearly uniform. Furthermore, the majority of the deformation of plates takes place near the plate boundaries, therefore in the calculations the stresses and strain-rates should be largest near the plate boundaries.

* Now at: Earth and Atmospheric Sciences, Purdue University, West Lafayette, IN 47906, USA.

† Now at: Department of Geological Science, University of Michigan, Ann Arbor, MI 48109, USA.

While this is a qualitative description, since we do not rigorously define what we mean by plate interior and plate boundary or how small the strain-rate in the interior of the plate should be, this broad definition will allow us to examine a wide range of 'plate-like' solutions. We can assess the effect that differences in the width of the deformation zone and the level of strain in the interior of the plate have on the overall flow. We point out that there are few observational constraints on the deformation of oceanic plates, and through numerical modelling we may be able to provide insight as to what observations would be most important for understanding plate–mantle interactions.

In the following sections we describe in detail three methods of modelling tectonic plates: the material property method (MP) implemented in a finite element code; the force balance method (FB) implemented in a spectral/finite difference code; and the power-law rheology method (PL) implemented in a finite difference code. With the grid sizes considered, the results from a constant viscosity Rayleigh–Benard benchmark problem using these three codes differ by less than 1 per cent (Travis *et al.* 1991).

Each method captures essential features of plate tectonics while ensuring that the plates do not artificially contribute to the kinetic energy of the system by actively driving or inhibiting convection. The effect of changing plate thickness as plates age is not included in defining the 'base' of the plate. Basal tractions are calculated at a constant depth. A more physical approach might be to calculate the tractions along an isotherm defining the mechanically strong part of the lithosphere. However neglecting this effect has a small effect on the outcome of the calculations. These methods do however include the important driving force due to the lateral temperature variations in the plate (Hager 1978; Hager & O'Connell 1981).

The methods described all produce surface velocities which, by the broad definition given above, are plate-like. We will use these methods to solve a simple set of problems, and comment on some of the differences between the methods. An important result is that all three methods agree not only qualitatively on the very broad features of the solution, but there is good agreement in quantitative details such as heat flux and surface velocity.

2 MODEL PROBLEM

We consider the simple geometry of a single plate across the top surface of a 2-D Cartesian box with free-slip, insulating side walls and a free-slip bottom. We choose an aspect ratio of 1.5 in order to produce a plate which is longer than the depth of the box, but still achieve a steady solution. The material property and force balance methods use a uniformly spaced, 49 by 33 node computational grid to eliminate differences in the solutions due to the grid resolution; however, it is necessary to use a 97 by 65 node grid for the power-law method to resolve the deformation in the non-Newtonian layer. The plate condition, which will be described in detail in the next section, is applied at the top of the box. In all three cases the plate is at a depth of 1/32th of the height of the box. The fluid has a constant viscosity, is heated from below and cooled from above with a Rayleigh number of 10^5.

A series of calculations is presented for each method. The properties of the plate are varied so that the plate velocity ranges from zero to values slightly greater than the average horizontal velocity of the bottom boundary. Each method varies different parameters to achieve this range of solutions.

In infinite Prandtl number convection, body forces are balanced by viscous forces and the net force on any mass element is zero. Similarly, the total force on a rigid plate is zero, although the tractions are non-zero on the ends and base of the plate. In two dimensions, the total force on a plate has a contribution from the basal shear tractions and from the normal stress on the ends of the plate (e.g., collisional resistance). The surface in contact with ocean or atmosphere is a traction free boundary. The changes in basal shear tractions must result in changes in normal tractions on the plate boundaries. We present all our results in terms of a dimensionless integrated shear traction on the base of the plate,

$$\hat{\tau} = \frac{\int_{L_{\text{plate}}} \tau_{xz}\, dS}{\int_{L_{\text{plate}}} \tau_{xz}^{\text{fixed top}}\, dS} \tag{1}$$

where L_{plate} is the length of the plate (in this case 1.5), τ_{xz} is the shear stress at the base of the plate, and $\tau_{xz}^{\text{fixed top}}$ is the shear stress at the same depth for a no-slip calculation.

We choose the following convention; $\hat{\tau} = 0$ implies that the plate driving force is completely supplied by the basal shear tractions with no force on the vertical bounding surfaces of the plate, $\hat{\tau} > 0$ implies that boundary forces are acting to resist plate motion and $\hat{\tau} < 0$ implies that the plate is moving faster than it would be if only the basal shear tractions were driving its motion and thus it is being aided by boundary forces. With this normalization, $\hat{\tau}$ is 0 for a plate whose motion is only due to shear traction on the base of the plate and 1 for a no-slip calculation (which is equivalent to a plate that cannot move).

The methods produced time-dependent solutions as $\hat{\tau}$ approached one. For computational reasons we did not attempt to obtain the value of the shear traction at which time dependence was first observed, but time-dependent solutions were observed for $\hat{\tau} > 0.8$. In order to simplify the comparisons, we only present results of steady solutions.

3 METHODS

3.1 Material property (MP)

The material property method uses *a priori* defined material property zones. The object of the material zones is to create plate-like behaviour through the variations in material properties within the plate. Weak zones are used to enhance deformation at the plate boundaries and a strong zone is used to minimize deformation within the plate. This is reasonable in light of what we know about mantle rheology: the lithosphere is cold, and due to temperature dependence, stronger than the interior of the mantle, while at plate boundaries the lithosphere may be weakened due to faulting and brittle failure or non-linear effects of stress on the rheology creating a lower effective viscosity (e.g., King & Hager 1990). The shape and viscosity of the material zones used in the computations can be chosen to match the

predicted rheology of the lithosphere (e.g., Ashby & Verrall 1977).

To minimize the impact of the weak zones on the rest of the solution, two-element by two-element squares are used for the weak zones at the plate boundaries. These zones are small compared to the size of the box ($D/16$ by $D/16$ where D is the depth of the box) so their impact on the flow should be minimal. The weak zones are located at the upper left- and right-hand corners of the computational domain. To make the rigid plate, a one-element-thick ($D/32$), high-viscosity zone along the top surface is used. This is much thinner than the boundary layer, but it is chosen to keep the calculation close to constant viscosity for comparison with the other methods. The viscosity changes discontinuously at the boundaries of the material zones. The only computational requirement on the sizes of these zones is that the depth of the weak zone be at least as deep as the thickness of the plate to avoid a situation where the plate locks up. Larger weak zones had only a minimal effect on the solutions. For this study a plate viscosity 10^3 times the interior viscosity is used. Previous work has shown that higher viscosities do not effect the solution (King & Hager 1990).

While it might appear that the viscosity of the weak zone is an unconstrained parameter, Fig. 1(a) shows that there is a direct mapping between the weak zone viscosity and the integrated basal shear traction, $\hat{\tau}$. This can be understood by considering the force balance on the plate. The shear tractions on the base of the plate must be balanced by the tractions on the ends of the plate. The stronger the weak zone becomes, the greater the end tractions on the plate become and the larger $\hat{\tau}$ becomes. As the weak zone viscosity decreases, the magnitude of $\hat{\tau}$ decreases. A negative shear traction occurs at the lowest viscosities because the traction balance on the weak zone requires that it exert a traction on the plate aiding plate motion, rather than opposing the plate motion as it does at higher viscosities. As Fig. 1(a) shows, $\hat{\tau}$ asymptotically approaches about one twentieth of the integrated basal shear traction for a no-slip calculation. However this value is dependent on the geometry of the weak zone.

3.2 Force balance (FB)

This method is described in detail, including the extension to three dimensions and multiple plates, in Gable (1989) and Gable *et al.* (1991). The approach is a constraint upon the geometry of surface plates. With the plate geometry defined, all forces acting on the plate and fluid are balanced to find the global velocity and stress fields which are consistent with the body forces and plate-like surface motion. For these calculations the plate geometry remains fixed, although the plate velocity, which is determined by balancing the forces on the plate, can be dependent. Computationally, the surface velocity is defined as zero at the endpoints and constant in the interior. The horizontal force balance on the plate is then

$$\int_{P_h} \tau_{xz}\, dS + \int_{P_v} \tau_{xx}\, dS = 0 \tag{2}$$

where P_h and P_v are the horizontal and vertical bounding surfaces of the plate, τ_{xz} is the shear traction due to convective flow across the base of the plate and τ_{xx} is the normal stress on the vertical plate boundaries. Calculating the tractions on the base of the plate (1/32th of the depth of the box) also avoids including the unphysical effect of a stress singularity at the plate boundary (e.g., Gable *et al.* 1991).

While the shear stress on the base of the plate is calculated directly from the flow field, the stress on vertical plate boundaries is parametrized as a fraction of the shear stress on the base of the plate, R, where

$$\int_{P_v} \tau_{xx}\, dS = R \int_{P_h} \tau_{xz}\, dS. \tag{3}$$

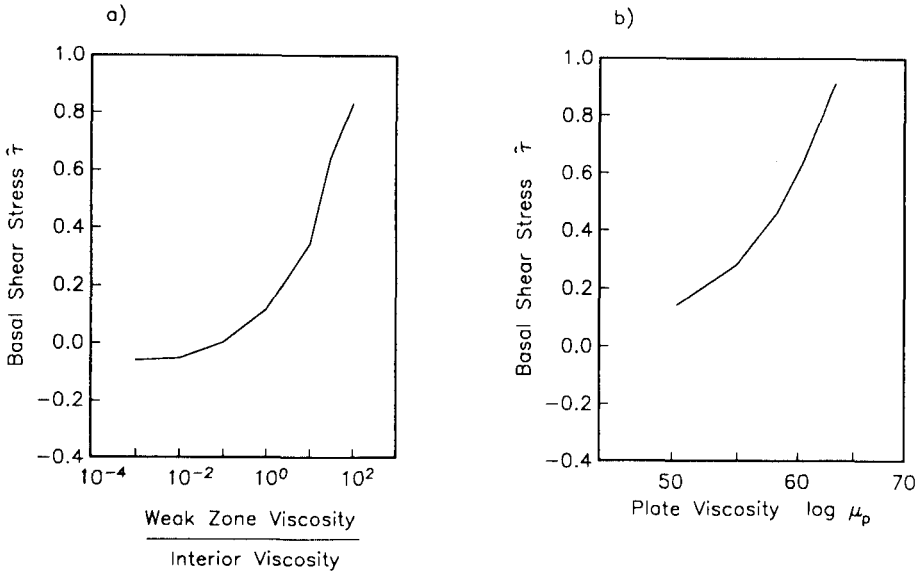

Figure 1. (a) The relationship between weak zone viscosity in the material property method (MP) and the normalized shear traction $\hat{\tau}$ from (1). (b) The relationship between the plate viscosity ($\log \mu_p$) and normalized shear traction $\hat{\tau}$ from (1) for a power-law exponent $n = 15$. $\hat{\tau}$ is 0 for a free-slip calculation and 1 for a no-slip calculation.

In this study, a suite of calculations are made where R, which acts as the plate strength at the boundaries, is varied from -0.25 to 1. When R is 1, the plate will be immobilized and is equivalent to a no-slip top boundary condition. When R is negative, $\hat{\tau}$ is negative.

3.3 Non-Newtonian rheology (PL)

Previous studies (Cserepes 1982; Christensen 1984) have shown that plate-like surface velocity profiles can be produced by convection in a non-Newtonian fluid layer. The success of these studies motivates the use of non-Newtonian rheology in this method.

The model consists of a thin, non-Newtonian layer with constant thickness situated on top of a thick Newtonian viscous layer (Weinstein 1991). The non-Newtonian layer represents the lithosphere and the Newtonian layer represents the mantle. D and h are the thicknesses of the Newtonian and non-Newtonian layers respectively and h/D is assumed to be $\ll 1$. Except for the difference in rheology, the two layers have identical properties. Convection in the Newtonian layer causes deformation in the non-Newtonian layer by generating shear tractions on the base of the non-Newtonian layer. For a large enough power-law exponent, the deformation in the non-Newtonian layer is concentrated in narrow regions.

The rheology of the non-Newtonian layer is assumed to be a powerlaw of the form

$$\tau_{xx} = 2\nu \frac{\partial u_p}{\partial x} \tag{4}$$

where

$$\nu = \mu_p (\tau_{xx})^{-(n-1)}, \qquad n = 1, 3, 5, \ldots . \tag{5}$$

In this expression, n is the power-law exponent, u_p is the horizontal velocity of the non-Newtonian layer, μ_p is a rheological constant with the dimensions of viscosity and τ_{xx} is the dimensionless normal stress. Only odd powers of n are considered so that the viscosity remains positive. The non-Newtonian layer is weak where the normal stresses are large and strong where the normal stresses are small. In the calculations presented in this study, the normal stresses are greatest at the ends of the non-Newtonian layer and thus give rise to weak zones at the plate boundaries and plate-like surface velocity profiles.

The non-Newtonian layer is coupled to the Newtonian layer by the dimensionless dynamic boundary condition

$$\tau_{xz} = h(2\mu_p)^{1/n} \left(\frac{\partial u_p}{\partial x}\right)^{1/n} \left(\frac{\partial u_p}{\partial x}\right)^{-1} \frac{\partial^2 u_p}{\partial x^2} \tag{6}$$

where τ_{xz} is the shear stress at the base of the non-Newtonian layer, x is the horizontal coordinate and h is the thickness of the non-Newtonian layer. The product of the first four terms in (6) is positive non-definite, therefore, the sign of the shear stress at the base of the non-Newtonian layer is the same as the sign of the curvature of the velocity distribution at that point. Since buoyancy forces in the non-Newtonian layer are not included, the thin non-Newtonian layer can never drive the flow. The relationship between the average shear traction and the plate viscosity (μ_p) is shown in Fig. 1(b) for a power-law exponent $n = 15$.

4 RESULTS

We present a comparison of results from the three different plate modelling methods. Three variables are used in the comparison, plate velocity, Nusselt number and the ratio of average surface velocity to average basal velocity. These variables are calculated as $\hat{\tau}$ varies between -0.25 and 1. In Fig. 2 we present surface velocity and topography profiles for the calculations closest to $\hat{\tau} = 0.64$ (recall that for MP and PL, $\hat{\tau}$ is an output and not specified). The topography is calculated from the vertical stress at the top of the box, following the method described in McKenzie *et al.* (1974). Notice that the interior velocities are uniform for all three methods and that the topography profiles are in excellent agreement.

Fig. 3(a) shows the average surface velocity, V_p, as a function of $\hat{\tau}$. For all three methods, there is not only an agreement in the trend of the velocities with the basal shear traction, but agreement to within 10 per cent in the

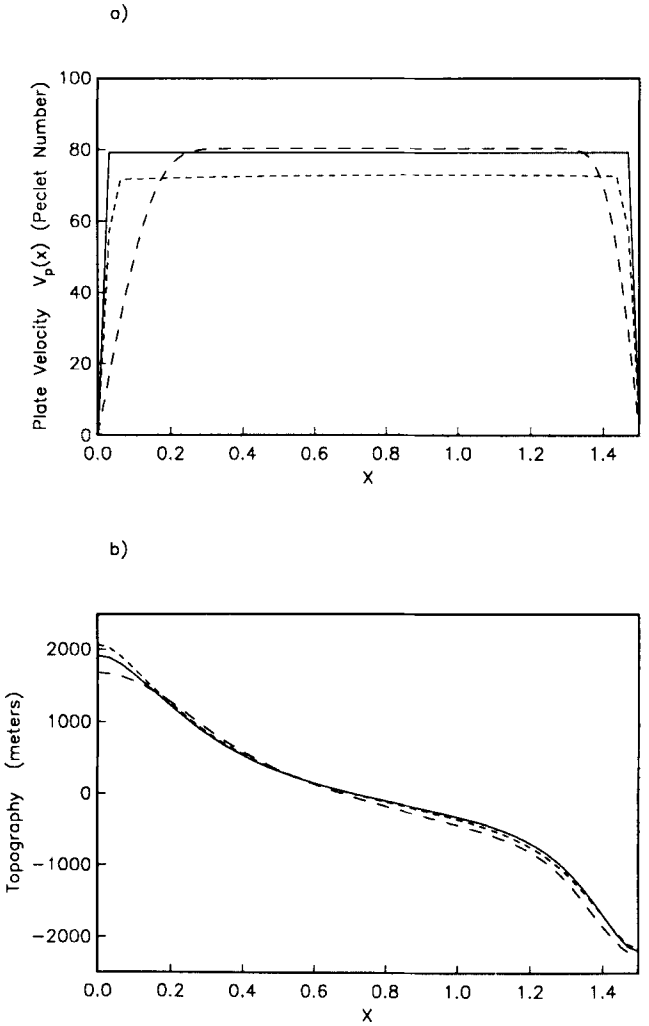

Figure 2. (a) Surface velocities for the force balance (solid line, $P = 0.96$), material property (short dashed line, $P = 0.96$), and power-law (long dashed line, $P = 0.8$) methods. For all three methods, the integrated basal shear traction is $\hat{\tau} = 0.64$. The velocities are plotted as Peclet numbers. (b) Topography profiles for the calculations in (a).

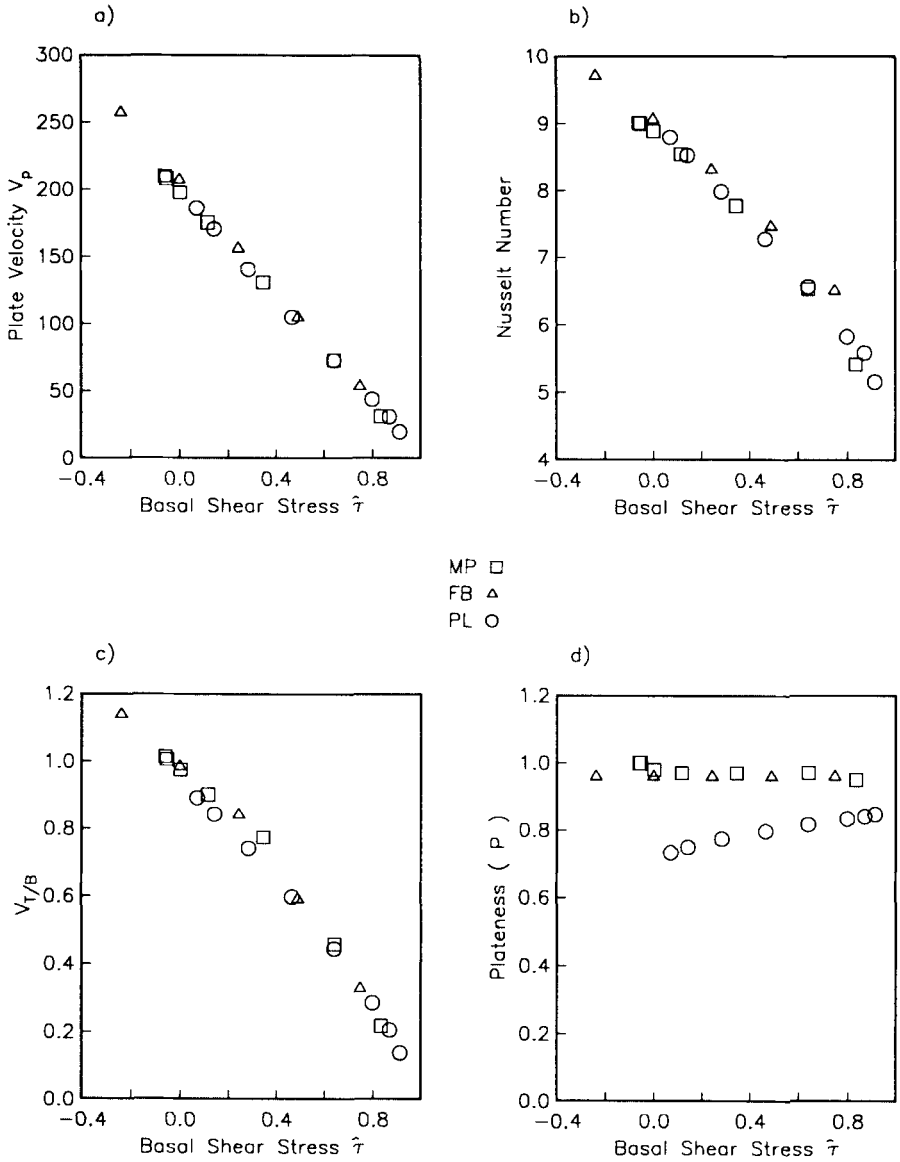

Figure 3. The (a) plate velocity, (b) Nusselt number, (c) $\bar{V}_{T/B}$ (ratio of plate velocity to bottom of the box velocity), and (d) P (plateness factor) for the three methods (squares—material property, triangles—force balance, circles—power law).

magnitude of the velocities. It is important to remember when interpreting these plots that each method is used with a different numerical method, so some slight differences in the solutions are expected due to the numerical approximations.

Next we examine the heat transport of the convective flow using the three methods. The Nusselt number is the ratio of the total heat flux across a fluid layer to its conductive value (Chandrasekhar 1961). Fig. 3(b) shows the Nusselt number as a function of the shear traction at the base of the plate ($\hat{\tau}$) for the three methods. Once again the three methods show good agreement.

To compare the plate velocity with the interior flow, we compare the ratio of the average surface velocity to the average basal velocity ($\bar{V}_{T/B}$):

$$\bar{V}_{T/B} = \frac{\int_{surface} v_x \, dl}{\int_{bottom} v_x \, dl}. \tag{7}$$

For a steady-state constant viscosity Rayleigh–Benard calculation, $\bar{V}_{T/B}$ is unity. Fig. 3(c) shows agreement among the methods similar to the agreement already shown for the Nusselt number and the plate velocity. Note that for calculations with a positive traction (where the end forces are opposing plate motion) $\bar{V}_{T/B}$ is less than unity, while for

calculations with a negative traction (where end forces are aiding motion), $\bar{V}_{T/B}$ is greater than unity.

To quantify the deformation of the plate, we define a 'plateness' parameter P,

$$P = \frac{1}{\pi - 2}\left[\pi - \frac{1}{L_{\text{plate}}}\int_0^{L_{\text{plate}}}\left|\frac{dU(x)}{dx}\right| dx\right] \quad (8)$$

where L_{plate} is the length of the plate and $U(x)$ is the horizontal velocity of the plate at the point x. The plateness parameter is a dimensionless number between zero and unity which provides a measure of the deformation of the plate. For a sinusoidal variation, P is zero, while for a boxcar function P is unity. For the force balance method, P is dependent only on the grid size (in these calculations P is 0.963). For the material property method, P is dependent on the size of the weak zone and is greater than 0.95 in all the calculations used in this study. For the power-law sheet method, P varies between 0.7 and 0.9 (see Fig. 3d). Therefore, the deformation across the plate varies from essentially no deformation ($P = 1$) to a continuous zone of deformation across the plate. The three methods agree equally well when they have similar values of $P(\hat{\tau} = 0)$ and when there is a large variation in $P(\hat{\tau} \rightarrow 1)$.

CONCLUSIONS

We find it quite remarkable that while the plate velocity and heat flux are nearly the same for all methods, the deformation of the plate exhibits differences (see Fig. 2). We believe this indicates that while these calculations are too simplistic to study the details of plate deformation, we are capturing the properties of plates which are important for studying global mantle flow. We point out that all our results are steady-state solutions, and that it is possible that for time-dependent solutions the deformation of the plate may play an important role in the formation of boundary layer instabilities or the pattern of flow.

We are encouraged by the overall agreement of these three, quite different methods on a simple problem. A criticism of plate modelling methods is that they are *ad hoc*. However, the scaling relations between these methods (Fig. 1) demonstrate that the material property and thin power-law sheet method satisfy basic physical principles by balancing the forces on the plate. They also provide a possible explanation for end forces on plates, namely changes in rheology. Furthermore, we show that it is possible to present plate results in geophysically understandable terms (i.e., basal plate tractions and collisional/extensional forces) rather than implementation specific parameters.

We also point out a need to be cautious, since the relationship between plate kinematics and convective flow is not completely understood. Also, our simplified models do not include a number of possibly important factors such as compositional differences between the plate and the asthenosphere, realistic plate/asthenosphere rheologies and elastic deformation within the plate. Our models are capable of producing a wide range of plate deformation patterns, and the details of plate deformation (particularly oceanic plates) are mostly unknown.

Based on the agreement in this study, we feel that all the methods presented successfully model a simple plate on the surface of a convecting fluid. We believe this comparison also demonstrates that the results are not dependent upon the plate modelling method and therefore are representative of the physical system we set out to model.

ACKNOWLEDGMENTS

This work is a result of discussions initiated at the Los Alamos National Laboratory Mantle Convection Workshop sponsored by the Institute of Geophysics and Planetary Physics and NSF. We thank U. Christensen, M. Gurnis, B. H. Hager and an anonymous reviewer for helpful comments. SAW acknowledges support from the UCRP of IGPP at LANL. SDK acknowledges support from the Green Foundation at IGPP Scripps Institution of Oceanography. CWG is jointly sponsored by NASA NAG5-840 and NSF EAR 86-18733 when at Harvard and work at LANL is performed under the auspicies of the US Department of Energy. Some calculations were performed at San Diego Supercomputer Center.

REFERENCES

Ashby, M. F. & Verrall, R. A., 1977. Micromechanisms of flow and fracture, and their relevance to the rheology of the upper mantle, *Phil. Trans. R. Soc. Lond.*, A, **288,** 59–95.

Chandrasekhar, S., 1961. *Hydrodynamic and Hydromagnetic Stability,* Oxford University Press, Oxford.

Christensen, U. R., 1984. Convection with pressure- and temperature-dependent non-Newtonian rheology, *Geophys. J. R. astr. Soc.*, **77,** 343–384.

Cserepes, L., 1982. Numerical studies of non-Newtonian mantle convection, *Phys. Earth planet. Inter.*, **30,** 49–61.

Davies, G. F., 1988. Role of the lithosphere in mantle convection. *J. geophys. Res.*, **93,** 10 451–10 466.

Davies, G. F., 1989. Mantle convection model with a dynamic plate: topography, heat-flow and gravity anomalies, *Geophys. J.*, **98,** 461–464.

Gable, C. W., 1989. Numerical models of plate tectonics and mantle convection in three dimensions, *PhD thesis,* Harvard University, Cambridge, MA.

Gable, C. W., O'Connell, R. J. & Travis, B. J., 1991. Convection in three dimensions with surface plates: Generation of toroidal flow, *J. geophys. Res.*, 8391–8405.

Gurnis, M., 1988. Large-scale supercontinents and the aggregation and dispersal of supercontinents, *Nature,* **332,** 695–699.

Gurnis, M. & Hager, B. H., 1989. Controls on the structure of subducted slabs and the viscosity of the lower mantle, *Nature,* **335,** 317–321.

Hager, B. H., 1978. Oceanic plate motions driven by lithospheric thickening and subducted slabs, *Nature,* **276,** 156–159.

Hager, B. H. & O'Connell, R. J., 1981. A simple global model of plate dynamics and mantle convection, *J. geophys. Res.*, **86,** 4843–4867.

Isacks, B. L., Oliver, J. & Sykes, L. R., 1968. Seismology and the new global tectonics, *J. geophys. Res.*, **73,** 5855–5899.

King, S. & Hager, B. H., 1990. The relationship between plate velocity and trench viscosity in Newtonian and power-law subduction calculations, *Geophys. Res. Lett.*, **17,** 2409–2412.

Kopitzke, U., 1979. Finite element convection models: Comparison of shallow and deep mantle convection and temperatures in the mantle, *J. Geophys.*, **46,** 97–121.

Le Pichon, X., 1968. Sea floor spreading and continental drift, *J. geophys. Res.*, **73,** 3661–3697.

McKenzie, D. P., Roberts, J. M. & Weiss, N. O., 1974. Convection

in the earth's mantle: towards a numerical simulation, *J. Fluid Mech.*, **62,** 465–538.

Morgan, W. J., 1968. Rises, trenches, great faults and crustal blocks, *J. geophys. Res.*, **73,** 1955–1982.

Nataf, H. C. & Richter, F. M., 1982. Convection experiments in fluid with highly temperature-dependent viscosity and the thermal evolution of the planets, *Phys. Earth planet. Inter.*, **29,** 320–329.

Richter, F. M. & McKenzie, D. P., 1978. Simple plate models of mantle convection, *J. Geophys.*, **44,** 441–471.

Travis, B. J., Anderson, C., Baumgardner, J., Gable, C., Hager, B. H., Olson, P., O'Connell, R. J., Raefsky, A. & Schubert, G., 1991. A benchmark comparison of numerical methods for infinite Prandtl number convection in two-dimensional Cartesian geometry, *Geophys. Astrophys. Fluid Dyn.*, **55,** 137–160.

Turcotte, D. L. & Oxburgh, E. R., 1967. Finite amplitude convective cells and continental drift, *J. Fluid Mech.*, **28,** 29–42.

Weinstein, S., 1991. Laboratory and numerical studies of dynamical processes related to thermal convection in the Earth's mantle, *PhD thesis,* The Johns Hopkins University, Baltimore, MD.